

Excited states in ^{52}Fe and the origin of the yrast trap at $I^\pi=12^+$

C. A. Ur,^{1,2} D. Bucurescu,² S. M. Lenzi,¹ G. Martínez-Pinedo,^{3,4} D. R. Napoli,⁵ D. Bazzacco,¹ F. Brandolini,¹ D. M. Brink,⁶ J. A. Cameron,⁷ E. Caurier,⁸ G. de Angelis,⁵ M. De Poli,⁵ A. Gadea,⁵ S. Lunardi,¹ N. Mărginean,² M. A. Nagarajan,⁹ P. Pavan,¹ C. Rossi Alvarez,¹ and C. E. Svensson⁷

¹*Dipartimento di Fisica and INFN, Sezione di Padova, Padova, Italy*

²*H. Hulubei Institute of Physics and Nuclear Engineering, Bucharest, Romania*

³*W. K. Kellogg Radiation Laboratory, California Institute of Technology, Pasadena, California*

⁴*Departamento de Física Teórica C-XI, Universidad Autónoma de Madrid, Madrid, Spain*

⁵*Laboratori Nazionali di Legnaro, INFN, Legnaro, Italy*

⁶*Dipartimento di Fisica and INFN, Trento, Italy*

⁷*McMaster University, Ontario, Canada*

⁸*Institut de Recherches Subatomiques, Strasbourg, France*

⁹*Department of Physics, UMIST, Manchester, United Kingdom*

(Received 10 November 1997)

Excited states in ^{52}Fe have been studied up to spin $10\hbar$ in the reaction $^{28}\text{Si}+^{28}\text{Si}$ at 115 MeV beam energy by using in-beam γ -ray spectroscopy methods at the GASP array. The excitation energy of the yrast 10^+ state is 7.381 MeV, almost 0.5 MeV above the well known β^+ -decaying yrast 12^+ state. Experimental upper limits for the $B(E4)$ transition probabilities from the 12^+ isomer to the 8_1^+ and 8_2^+ states have been determined. The mean lifetimes of five excited states have been measured by using the Doppler shift attenuation method. Complete diagonalizations in the pf major shell lead to very good agreement with the experimental level scheme and transition probabilities. The lifetime, $\log ft$ value, branching ratios, and $B(E4)$ values are calculated for the 12^+ isomer. The positive parity states are also interpreted in terms of a Nilsson projected method. The structure of the yrast levels of ^{52}Fe is compared with those of its cross conjugate ^{44}Ti .
[S0556-2813(98)02610-7]

PACS number(s): 21.10.Tg, 21.60.Cs, 23.20.Lv, 27.40.+z

I. INTRODUCTION

Recently, the study of the $f_{7/2}$ -shell nuclei has gained renewed interest. The development of very efficient detector arrays both for γ rays and charged particles has allowed investigations of the structure of these nuclei at higher spins than heretofore possible [1–3]. Nuclei near the middle of the $f_{7/2}$ shell show strong collective behavior near the ground state [4]. At higher spins, shape transitions towards triaxial and noncollective deformations can occur due to an intimate interplay between the collective and microscopic degrees of freedom. Recently, band terminating states, corresponding to fully aligned $f_{7/2}$ configurations, were observed in ^{48}Cr [2] and ^{50}Cr [3]. When approaching the doubly magic nucleus ^{56}Ni the collective behavior is rapidly disappearing as nuclei evolve towards a spherical shape.

So far, the nucleus ^{52}Fe has been an experimental challenge. Most of the known excited states in this nucleus are of relatively low spin (below $6\hbar$) and have been observed in ($^3\text{He},n$) [5–7], ($\alpha,2n$) [8], and (p,t) [9] reactions (see also Ref. [10]). Attempts to extend the ^{52}Fe yrast structure to higher spins in fusion-evaporation reactions induced by heavy ions have failed so far (see Refs. [11,12], and references therein). Higher spin states in ^{52}Fe are obscured by the presence of a 12^+ isomer at 6.82 MeV excitation energy, which acts to “trap” and divert the deexciting γ -ray flux to the neighboring nucleus ^{52}Mn [12,13]. With the large γ -ray detector arrays now available, previously undetected high-spin states around and below the isomer can be observed and studied.

In this work, performed with the GASP [14] detector array, we have been able to extend the level scheme of ^{52}Fe up to the 10^+ state, thereby confirming the predicted inversion [12,13] of the yrast 10^+ and 12^+ states. The experimental data have been interpreted in the framework of the spherical shell model (SM) in the full pf shell. The intrinsic structure of the states has been investigated by using a Nilsson projected method.

II. EXPERIMENTAL DETAILS

High spin states in the nucleus ^{52}Fe were populated via the $^{28}\text{Si}+^{28}\text{Si}$ reaction at 115 MeV beam energy. The silicon beam was delivered by the XTU Tandem accelerator at the National Laboratory of Legnaro. The target consisted of ~ 0.8 mg/cm² ^{28}Si (enriched to $>99.9\%$) evaporated on a 13 mg/cm² Au backing. γ rays were detected with the GASP array which consists of 40 Compton-suppressed large volume HP Ge detectors and an inner ball of 80 BGO crystals. The 40 Ge detectors are placed symmetrically relative to the beam axis in seven rings as follows: six detectors at 35° , six detectors at 60° , four detectors at 72° , eight detectors at 90° , four detectors at 108° , six detectors at 120° , and six detectors at 145° . Data were recorded when at least two Ge detectors and two elements of the BGO inner ball fired in coincidence. A total of 7.8×10^8 twofold and 5.4×10^7 threefold events were collected. Gain matching and efficiency calibration of the Ge detectors were performed using ^{152}Eu and ^{56}Co radioactive sources. The total fusion cross section of the reaction is fragmented in a large number of channels.

To estimate the relative yield of these channels we used a total γ - γ coincidence matrix in which we determined the intensities of the γ -ray transitions feeding the ground states. The most intense channels populated in our reaction were ^{50}Cr ($\alpha 2p$) with $\sim 31\%$, ^{49}Cr ($\alpha 2pn$) with $\sim 29\%$, and ^{49}V ($\alpha 3p$) with $\sim 11\%$ of the total fusion cross section whereas the population of the ^{52}Fe ground state was estimated to represent less than 1%. States in ^{52}Fe were populated either by $2p2n$ or α evaporation.

III. DATA ANALYSIS

A. The level scheme

Previous studies of ^{52}Fe [7,9,12,15] have established the position of the yrast 2^+ , 4^+ , 3^- , and 5^- states, of a second 4^+ state, and of the long lived yrast 12^+ state. This isomeric level, placed at an excitation energy of 6820 ± 130 keV and with a measured half-life of 45.94 ± 0.60 sec [12], decays primarily by β^+ emission towards ^{52}Mn . An upper limit of 0.4% was established [12] for the γ decay of the 12^+ state.

The high efficiency of the GASP array allowed us to identify new γ -ray transitions belonging to ^{52}Fe by setting gates on the previously known γ rays. Double gated γ -coincidence spectra with gates set on some key transitions assigned to ^{52}Fe are shown in Fig. 1. On the basis of such γ - γ coincidence data obtained from a γ - γ - γ coincidence cube and of the relative intensities of the transitions, we have constructed the level scheme shown in Fig. 2. The relative intensities of the transitions were extracted from the 90° spectrum in coincidence with the 850 keV $2^+ \rightarrow 0^+$ transition in order to avoid the uncertainties introduced by the line shape broadening. The intensity for the 2753 keV transition which is assumed to be of $\Delta I = 1$ character (see level scheme) is already corrected for the angular distribution as specified in Ref. [16]. The high energy part of the spectrum at 90° in coincidence with the 850 keV transition, from which the relative intensities were extracted, is shown in Fig. 3.

The yrast 6^+ state suggested in Ref. [7] is confirmed; furthermore a new 6^+ state as well as two 8^+ states and a 10^+ state lying at 7.381 MeV, well above the 12^+ β^+ -decaying isomer, are established. This constitutes the first direct observation of the predicted [12] inversion between the yrast 10^+ and 12^+ states. Three new γ rays connecting the 5^- level with the 3^- , 4_1^+ , and 4_2^+ states were identified. High spin states in ^{52}Fe have also been identified in a parallel experiment performed recently at Gammasphere [17].

Spins and parities were assigned on the basis of the angular distribution of the γ rays. Data were sorted into two γ - γ coincidence matrices having on one axis γ rays detected at all angles and on the second axis those detected at 60° or 120° and those detected at 90° , respectively. By setting gates on the axis with all the detectors, the intensity of the observed γ rays follows the regular angular distribution law disregarding the multipole character of the gating transition. The ADO (angular distribution from oriented states) ratio is defined as [18]

$$R_{\text{ADO}} = \frac{[I_\gamma(\theta) + I_\gamma(180^\circ - \theta)]/2}{I_\gamma(90^\circ)}, \quad (1)$$

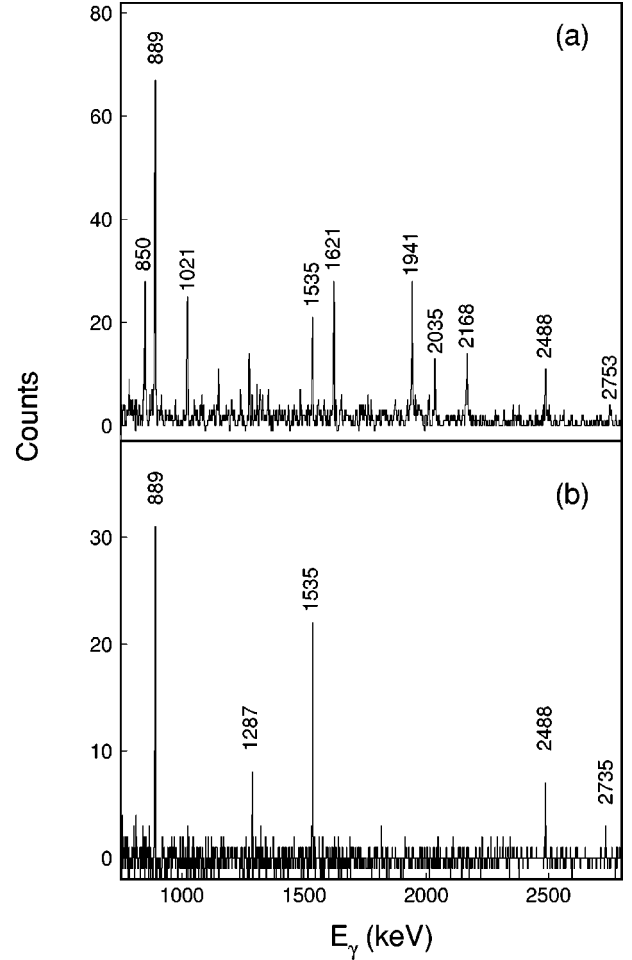


FIG. 1. Examples of double-gated spectra for some selected transitions assigned to ^{52}Fe . (a) Gates set on the first two yrast transitions, $2_1^+ \rightarrow 0_1^+$ and $4_1^+ \rightarrow 2_1^+$. The contaminant peaks between 1021 and 1535 keV belong to the strong channel ^{47}V . (b) Gates set on the $2_1^+ \rightarrow 0_1^+$ and $8_2^+ \rightarrow 6_2^+$ transitions.

where I_γ denotes the intensity of the observed γ ray at the angles θ , $180^\circ - \theta$, and 90° , respectively, corrected by the detection efficiency. Typical values of the ADO ratios for $\theta = 60^\circ$ in the GASP geometry are ~ 1.17 for a stretched quadrupole transition and ~ 0.85 for a stretched dipole transition. The γ -ray energies and relative intensities of the transitions belonging to ^{52}Fe , together with their ADO ratios at 60° and spin-parity assignments, are reported in Table I. Spin and parity of the new levels are based on ADO analysis, by assuming that transitions with $R_{\text{ADO}} \approx 1.17$ have stretched $E2$ character. The results for the 1941, 2168, and 889 keV transitions lead therefore to $I^\pi = 10^+$ for the state at 7.381 MeV.

We could not extract the angular distribution of the 2735 and 2753 keV γ -ray transitions depopulating the 4_2^+ and 5^- states, respectively, since their broadened line shapes are overlapping. The spin assignment for the states decaying via these two transitions are based on previous measurements. In Ref. [7] the angular distribution of the 2735 keV transition was found to be compatible with an $E2$ character. This assignment is now supported by the observation of a 1286 keV transition connecting the 6_2^+ state to the 4_2^+ state. A level at 5138 ± 4 keV excitation energy decaying towards the 4^+

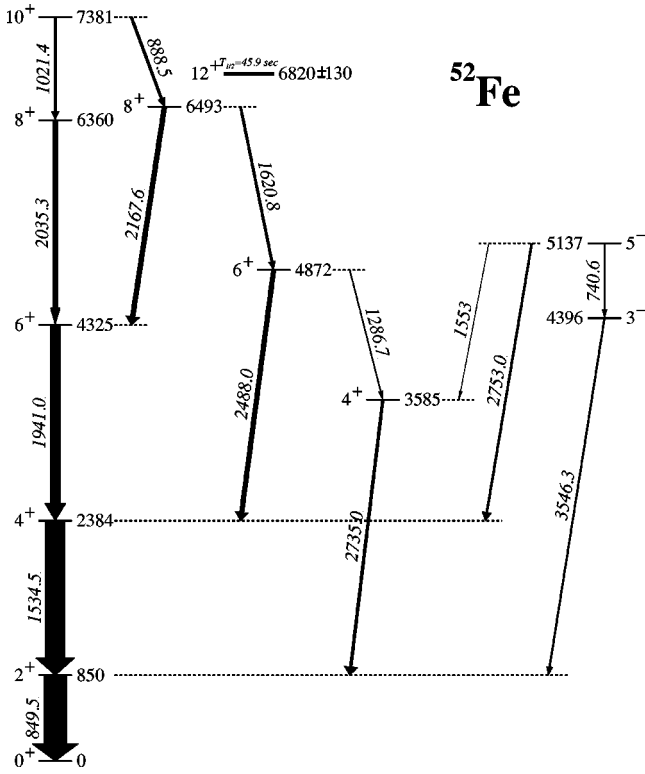


FIG. 2. Level scheme of ^{52}Fe , as obtained in the present experiment. The excitation energy and lifetime of the 12^+ β^+ -decaying isomeric state is taken from Ref. [12].

yrast state was also reported in Ref. [7]; later on [9], a 5^- assignment was given to that state. This implies $\Delta I=1$ character for the new measured γ -ray transitions of 1553 and 2753 keV. The 5^- assignment is also confirmed by the $E2$ character of the 740 keV γ ray feeding the 3^- state.

The determination of the excitation energies of the two 8^+ levels now allows a better estimation of the $B(E4)$ values for the γ decay of the 12^+ isomer, by using the upper limit of 0.4% for the total γ -ray branching determined in the off-beam measurement of Ref. [12]. For each of the two possible $E4$ transitions (towards 8_1^+ and 8_2^+ states) we get

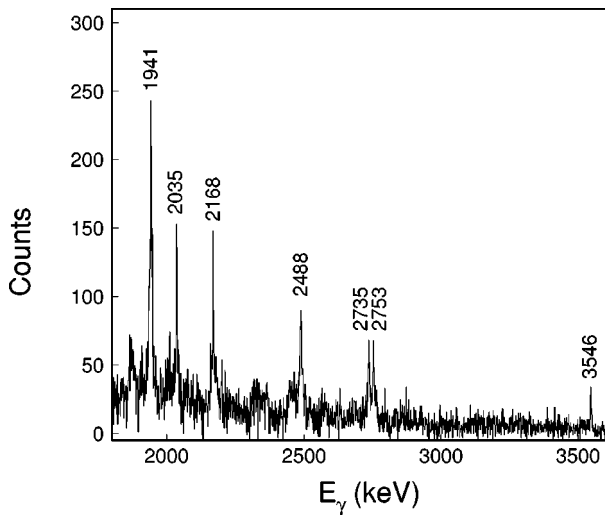


FIG. 3. High-energy γ -ray spectrum at 90° in coincidence with the 850 keV transition.

TABLE I. Relative intensities, ADO ratios, and spin assignments in ^{52}Fe .

E_γ (keV)	Intensity ^a	ADO ratios ^a	Assignment
740.6	5.5(6)	1.27(11)	$5^- \rightarrow 3^-$
849.5			$2^+ \rightarrow 0^+$
888.5	11.5(8)	1.20(8)	$10^+ \rightarrow 8_2^+$
1021.4	13.1(25)		$10^+ \rightarrow 8_1^+$
1286.7	5.0(10)		$6_2^+ \rightarrow 4_2^+$
1534.5	100.0(6)	1.16(4)	$4_1^+ \rightarrow 2^+$
1553	1.0(5)		$5^- \rightarrow 4_2^+$
1620.8	13.6(26)		$8_2^+ \rightarrow 6_2^+$
1941.0	55.0(30)	1.15(6)	$6_1^+ \rightarrow 4_1^+$
2035.3	21.0(30)	1.46(18)	$8_1^+ \rightarrow 6_1^+$
2167.6	20.7(20)	1.24(11)	$8_2^+ \rightarrow 6_1^+$
2488.0	21.9(15)	1.34(19)	$6_2^+ \rightarrow 4_1^+$
2735.0	15.0(17)		$4_2^+ \rightarrow 2^+$
2753.0	10.0(20)		$5^- \rightarrow 4_1^+$
3546.3	7.0(15)	0.92(8)	$3^- \rightarrow 2^+$

^aValues are extracted from spectra in coincidence with the 850 keV $2^+ \rightarrow 0^+$ transition.

now the following upper limits:

$$B(E4; 12^+ \rightarrow 8_1^+) < 379 \text{ e}^2 \text{ fm}^8 \text{ (0.16 W.u.)},$$

$$B(E4; 12^+ \rightarrow 8_2^+) < 8360 \text{ e}^2 \text{ fm}^8 \text{ (3.53 W.u.)}. \quad (2)$$

These values do not include the large uncertainty (130 keV) in the excitation energy of the 12^+ state [12]. They are in the range of other experimental $B(E4)$ values determined in pf -shell nuclei, such as 1.42(5) W.u. in ^{44}Sc , 0.146(4) W.u. in ^{52}Mn , and 0.256(6) W.u. in ^{53}Fe [19].

B. DSAM analysis

To perform the analysis of the Doppler broadened line shapes we sorted the data in seven $4k \times 4k$ γ - γ -coincidence matrices, each corresponding to the coincidence between the detectors of one ring and all other detectors. We have analyzed the γ -ray spectra in coincidence with the 850 keV γ ray (which does not show any appreciable broadening) in order to select better the channel of interest and to reduce as much as possible the contaminations on the line shapes of the relevant transitions.

The $10^+ \rightarrow 8_1^+$ and $10^+ \rightarrow 8_2^+$ γ -ray transitions do not exhibit a broadened line shape, indicating that the 10^+ state has a long lifetime. Changes in the line shape for lower states were observed only when a large amount of side feeding was present (see Table I).

The lifetime analysis was carried out with the computer code LINESHAPE [20]. The slowing down process and the scattering of the recoils in the target and in the backing were described by a Monte Carlo simulation [21], with a modification regarding the spread in the initial direction of the recoils due to the evaporation of light particles [22]. The simulation was performed with 5000 histories and up to 187 time steps covering the recoil range in the backing. Northcliffe and Schilling [23] electronic stopping power values have been used in the calculations.

The program performs a χ^2 minimization of the line shape fit as a function of the level lifetime, the side-feeding time, and the normalization factors. We used a one step side-feeding for each level, the side-feeding intensity being a fixed parameter in the program. The background and the intensity of contaminant peaks present in the spectra were kept fixed. The analysis was done for each line separately starting with the highest transition in the level scheme. Line shapes were fitted at forward and backward angles simultaneously allowing a better identification of the contaminants. The program, designed to deal with cascades of γ rays connecting states with side-feeding originating only from the continuum, is not suited for level schemes such as that of ^{52}Fe . However, it could still be used by properly transforming the complex feeding scheme into equivalent γ -ray cascades.

We determined first the lifetimes of the two 8^+ states from the analysis of the two decay branches $10^+ \rightarrow 8_1^+ \rightarrow 6_1^+$ and $10^+ \rightarrow 8_2^+ \rightarrow 6_1^+$, respectively. The lifetime of the yrast 6^+ state was extracted by analyzing the decay pattern along the yrast sequence. To account for the feeding provided via the decay of the 8_2^+ state, we introduced above the 6_1^+ state a virtual level with zero lifetime and side-feeding time given by the lifetime of the 8_2^+ state. The intensity of the 1021 keV transition was modified to account for the whole long-lived population of the 6_1^+ level provided by the decay of the 10^+ state. The lifetime of the second 6^+ state was extracted from the analysis of the sequence of γ -ray transitions $10^+ \rightarrow 8_2^+ \rightarrow 6_2^+ \rightarrow 4_1^+$. In order to describe the multiple feeding of the 4_1^+ state, we have again introduced virtual levels of mean lifetime equal to zero and side-feeding times given by the lifetimes of the 6_2^+ and 5^- states, respectively.

In Fig. 4 the best fits for the line shapes (measured at 72°) of several γ -ray transitions are displayed. The line shape of the 2035 keV transition is strongly contaminated by the presence of the 2045 keV line belonging to ^{49}Cr with a very pronounced line shape. We determined the lifetime of the 8_1^+ state from the best fit of the experimental spectrum with that obtained after summing the calculated line shape of the 2035 keV γ -ray transition and the experimental line shape of the contaminant line.

The line shapes of the 2735 and 2753 keV transitions overlapped and consequently a definite lifetime value for the 4_2^+ and 5^- states could not be extracted. A lower limit of about 1 ps was estimated for the side feeding of the 4_1^+ provided via the 2753 keV transition. Variation of this side feeding time in the range 0.5–2.0 ps has no practical effect on the mean lifetime value of the 4_1^+ state.

The results are reported in Table II together with previous measured values. The experimental reduced transition probabilities $B(E2)$ have been extracted according to the expression [24]

$$B(E2)(e^2 \text{ b}^2) = \frac{0.08156 B_\gamma}{\tau E_\gamma^5 (1 + \alpha_{\text{tot}})}, \quad (3)$$

where B_γ is the branching ratio of the γ -ray transition, τ is the lifetime of the state in picoseconds, E_γ is the energy of the transition in MeV, and α_{tot} is the total conversion coef-

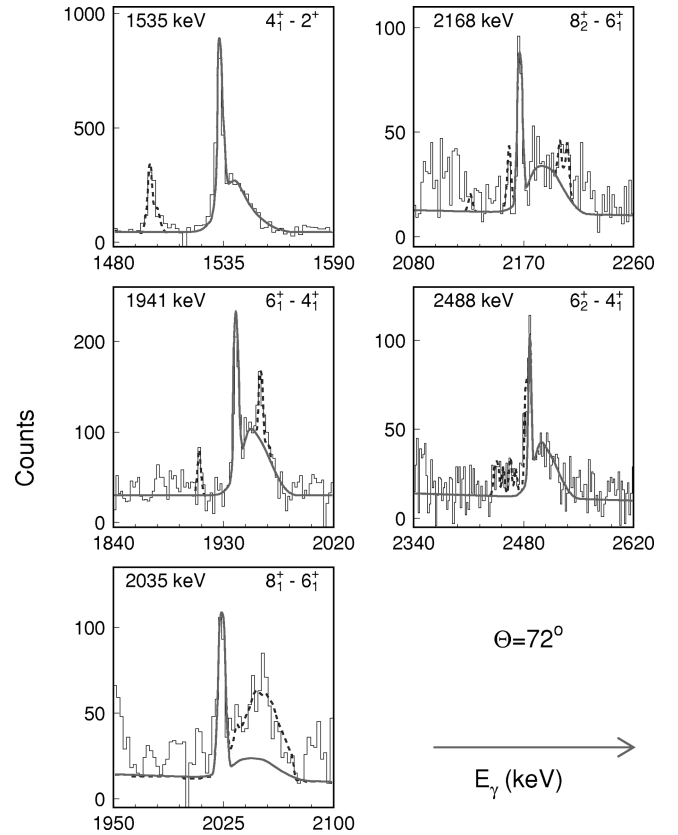


FIG. 4. Doppler broadened line shapes for the transitions of 1535 keV ($4_1^+ \rightarrow 2_1^+$), 1941 keV ($6_1^+ \rightarrow 4_1^+$), 2035 keV ($8_1^+ \rightarrow 6_1^+$), 2168 keV ($8_2^+ \rightarrow 6_1^+$), and 2488 keV ($6_2^+ \rightarrow 4_1^+$), at 72° . Full lines show least square fits performed with the LINESHAPE program and correspond to the mean lifetime values reported in Table II. The contaminant peaks are indicated by dashed lines.

ficient ($\alpha_{\text{tot}} \approx 0$ in this case). These $B(E2)$ values are compared to the ones calculated within the SM (see Sec. IV A).

IV. DISCUSSION

Nuclei which lie in the middle of the $f_{7/2}$ shell are strongly deformed near the ground state. This allows application of different models for the description of their nuclear structure. Aside from the shell model, one can also interpret these nuclei in terms of an intrinsic deformed state. These studies have been performed for instance in ^{48}Cr , which has the maximum number of valence $f_{7/2}$ nucleons to develop deformation in this mass region [25]. Nuclei such as ^{52}Fe , which are not as close to the middle of the shell, are less deformed and the incipient rotational behavior at low spin rapidly smears out with increasing angular momentum, due to the interplay between collective and single particle degrees of freedom.

In the vicinity of closed shells, excited nuclear states are explained in terms of rearrangement of the nucleons in the available single particle orbitals. This usually results in irregular decay patterns, isomeric states, and yrast traps. The isomeric 12^+ state in ^{52}Fe represents an energy-spin yrast trap due to its large spin difference from all the lower energy states [26].

In addition to $^{52}\text{Fe}^m$, several high spin yrast traps have

TABLE II. Mean lifetimes of ^{52}Fe states from the present analysis and a previous study compared with the SM calculations.

E_x (keV)	E_γ (keV)	I_i	I_f	τ (ps)		τ_{SF} (ps) ^a	$B(E2)$ ($e^2 \text{fm}^4$)	
				previous work [12]	present work		Exp.	SM
850	849.5	2	0	>1.0			<1844 ^b	154.5
2384	1534.5	4 ₁	2	0.40 ^{+0.29} _{-0.14}	0.32±0.08	0.06 ^{+0.03} _{-0.02}	300±69	223.5
4325	1941.0	6 ₁	4 ₁		0.24±0.08	0.04 ^{+0.02} _{-0.01}	124±40	117.9
4872	2488.0	6 ₂	4 ₁		0.30±0.12	0.04 ^{+0.03} _{-0.02}	29±14	83.3
6360	2035.3	8 ₁	6 ₁		0.21±0.08	0.01 ^{+0.01} _{-0.01}	74±25	85.6
6493	2167.6	8 ₂	6 ₁		0.26±0.06	0.01 ^{+0.01} _{-0.00}	43±15	11.3

^aStatistical errors are specified.

^bValue calculated on the basis of the experimental limit given in Ref. [11].

been identified along the periodic table but few of them originate through the inversion in energy with yrast states of lower spins. Such yrast traps have been observed in ^{53}Fe [27], ^{53}Co [28], ^{156}Hf [29], ^{211}Po [30], and ^{212}Po [31]. The nature of the energy-spin yrast traps can be related to the alignment of nucleons [12]. The nucleons with aligned spins gain energy because their residual interaction is stronger for wave functions with large spatial overlap (MONA effect [32]). In most of the cases the structure of these states is associated with oblate deformation or ‘‘single particle’’ rotations [26]. A different structure is found in ^{52}Fe , where the effect of the maximum alignment is accompanied by a quadrupole coherence that produces a prolate deformation at $I = 12\hbar$. This will be discussed in the next subsections.

A. Shell model calculations

The structure of ^{52}Fe has been analyzed in the framework of the spherical shell model in the full pf shell. The m -scheme dimension, 109,954,620, is the largest attained so far. Previous calculations [25,33,34] reproduce with good accuracy the experimental data of the nuclei in this mass region [2,3]. Here the KB3 effective interaction [35] was used, with single particle energies taken from the experimental spectrum of ^{41}Ca . The effects of core polarization on the quadrupole properties were taken into account by using the usual effective charges, $e_\pi = 1.5$ and $e_\nu = 0.5$. The Hamiltonian was treated by the Lanczos method and diagonalized with the code ANTOINE [36]. The resulting theoretical level scheme is compared in Fig. 5 with the experimental one. Fairly good agreement is found, with a root-mean-square deviation for the yrast levels of 175 keV. The energy inversion of the 12^+ isomeric state with the 10^+ yrast is reproduced theoretically, although the energy gap between the two states is smaller than in the experiment.

A good reproduction of the energy spectrum is not enough to establish the quality of the shell model calculations. A more stringent test is their ability to reproduce the experimental lifetimes and the $B(E2)$ values. The calculated $B(E2)$ values for ^{52}Fe are displayed in Table II. They are in good agreement with the experimental ones. The poorer concordance for the second 6^+ and 8^+ states may be due to the presence of nearby states of the same spin and parity (see Fig. 2).

The shell model calculations provide also the static electric quadrupole moments Q , which are plotted in Fig. 6.

Large negative values are obtained for the first two excited states. As already pointed out in Ref. [37], ^{52}Fe behaves as a rotor below $I = 6\hbar$, consistently with a $K = 0$ band. Using the rotational model prescription we obtained for the lowest 2^+ and 4^+ states an intrinsic quadrupole moment $Q_0 \approx 90e \text{fm}^2$ from both the theoretical $B(E2)$ values and the quadrupole moments. The deduced deformation parameter is $\beta = 0.23$. At $I = 6\hbar$, Q changes sign and becomes very small. This change of regime can be related to the process of particle alignment, since the mechanism of generating angular momentum by aligning the valence-particle spins along the rotational axis in a high- j shell becomes energetically favored at high frequency.

In Fig. 7, the experimental yrast bands of the even-even $N = Z$ nuclei ^{44}Ti , ^{48}Cr , and ^{52}Fe are shown up to the maximum spin that can be built in the $f_{7/2}$ shell. The nucleus ^{48}Cr is presented to stress the evolution of the collectivity along

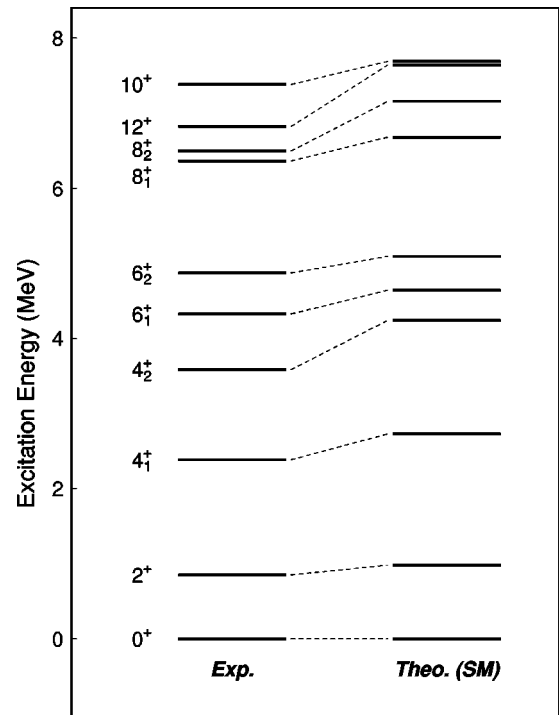


FIG. 5. Comparison between the experimental and the shell model positive parity energy levels in ^{52}Fe . Dashed lines connect the experimental levels with their calculated counterparts.

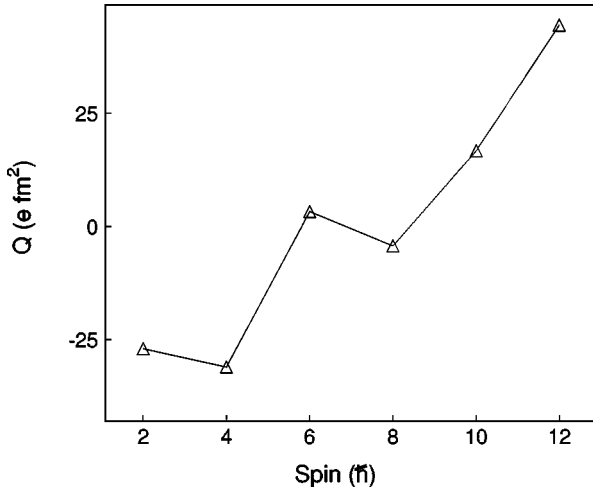


FIG. 6. The electric quadrupole moments of the yrast states in ^{52}Fe obtained with full pf spherical shell model calculations.

the $N=Z$ line. The cross conjugate nuclei ^{52}Fe and ^{44}Ti should have the same energy spectra in the simple $(f_{7/2})^n$ model. In fact, the two level schemes are quite similar at low spin. However, the symmetry is broken at high spin: there is no inversion of the 10^+ and 12^+ states in ^{44}Ti . This effect was discussed in Ref. [12] within the $(f_{7/2})^n$ model but using different effective interactions for the two nuclei. In the present analysis, the SM calculations treat all nuclei in the $f_{7/2}$ shell on the same footing. In this way, one can follow the evolution of the microscopic structure with the spin.

The fractional occupation numbers of the $f_{7/2}$, $p_{3/2}$, $f_{5/2}$, and $p_{1/2}$ orbitals are plotted for the yrast states of ^{52}Fe in Fig. 8. For comparison, the same quantities are also reported for its cross conjugate nucleus ^{44}Ti and for the most quadrupole deformed nucleus in the $f_{7/2}$ shell ^{48}Cr . Although from a qualitative observation of Fig. 8 the $f_{7/2}$ subshell is by far the most occupied one, the contribution arising from the rest of the orbitals in the pf shell becomes crucial in obtaining a good description of these nuclei.

Recently, it has been shown [38] that the development of quadrupole coherence that gives rise to rotational-like bands

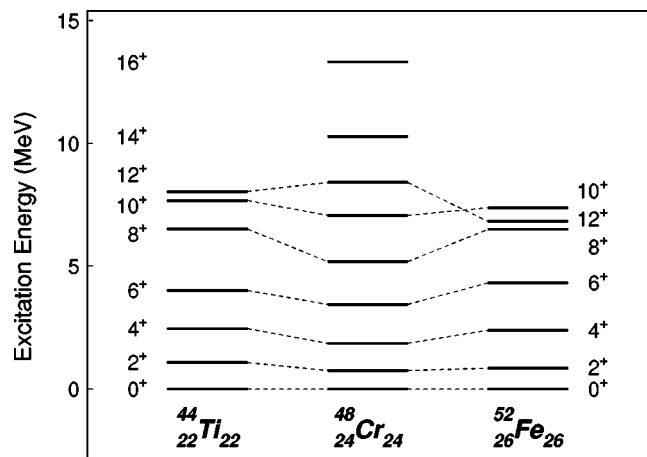


FIG. 7. Experimental yrast states in the cross-conjugated nuclei ^{44}Ti and ^{52}Fe and in the self-conjugated nucleus ^{48}Cr showing the evolution of the collectivity along the $N=Z$ line in the $f_{7/2}$ shell.

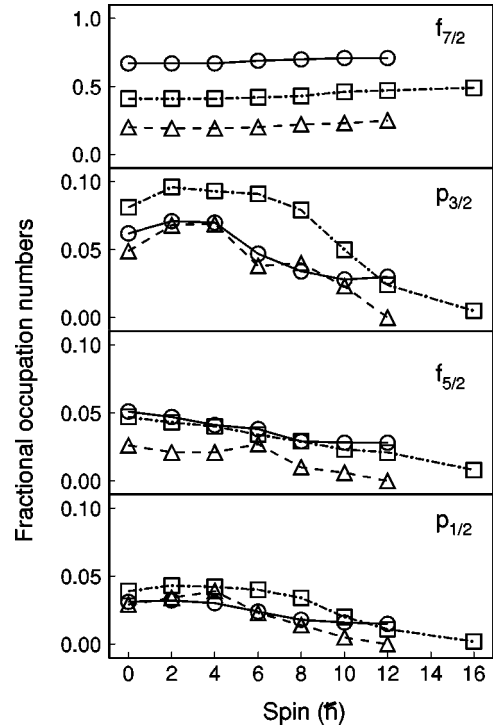


FIG. 8. The fractional occupation numbers of specific orbitals in the pf shell for the yrast even spin states in ^{44}Ti (triangles), ^{48}Cr (squares), and ^{52}Fe (circles) as extracted from the SM calculations.

in these nuclei, comes from the mixing of the $f_{7/2}$ and $p_{3/2}$ orbitals. In all three nuclei, the $p_{3/2}$ occupation number remains almost constant at low spin. The largest contribution occurs in the most deformed nucleus ^{48}Cr . There it decreases monotonically above the backbending ($I=10\hbar$) as do the other two components ($f_{5/2}$ and $p_{1/2}$). In ^{52}Fe and ^{44}Ti , this happens at much lower spin, $I=6\hbar$.

At the maximum spin that can be constructed with the valence particles in the $f_{7/2}$ shell, the $p_{3/2}$, $f_{5/2}$, and $p_{1/2}$ occupation numbers vanish for ^{44}Ti ($I=12\hbar$) and become insignificant for ^{48}Cr ($I=16\hbar$). The $f_{7/2}$ becomes the only relevant orbit. These fully aligned band-terminating states are of noncollective character. The situation is different in ^{52}Fe , where above $I=6\hbar$, all contributions remain almost constant as a function of spin, even at $I=12\hbar$. This residual collectivity in the 12^+ state can be related to the energy inversion of the 10^+ and 12^+ states, which gives rise to the yrast trap.

B. Nilsson calculations

The change of regime at $I=6\hbar$, reflected in the fractional occupation numbers and in the electric quadrupole moments obtained from the shell model in the previous subsection, can be related, in the language of the rotational model, to a crossing between the ground state $K=0$ band and an excited $K=6$ band. To study this problem we have computed different Nilsson intrinsic states and projected them onto good angular momentum. The $K=0$ band corresponds to an intrinsic state obtained by filling the $[330]1/2$, $[321]3/2$, $[312]5/2$ Nilsson orbitals for protons and neutrons. The intrinsic state of the $K=6$ band is constructed by exciting one proton *or* one neutron from the $[312]5/2$ to the $[303]7/2$ orbital. Our calcula-

tions indicate that the $I=6, K=6$ and the $I=6, K=0$ states are degenerate. This also explains the presence of two 6^+ levels close in energy (see Fig. 2). The states between 6_1^+ and 10^+ could be thus considered as a mixing of a $K=0$ band with a $K=6$ band. We cannot speak of a well defined intrinsic state.

This procedure was repeated for the state at $I=12\hbar$, where there is a residual quadrupole coherence. A $K=12$ intrinsic prolate Nilsson state can be constructed by exciting two particles, a proton *and* a neutron, from the $[312]5/2$ to the $[303]7/2$ orbit. After projecting this state onto good angular momentum, an overlap of ~ 0.9 with the exact shell model wave function of the 12^+ state is obtained. The excitation energy of this level is lower than the $I=10\hbar$ and $I=12\hbar$ states coming from the $K=0$ and $K=6$ bands, which explains the presence of the yrast trap.

It is interesting to note that in addition to ^{52}Fe , the mirror nuclei ^{53}Fe and ^{53}Co have yrast traps at $I^\pi=19/2^-$ [27,28]. The structure of these nuclei is well reproduced by our shell model calculations. We have also performed Nilsson projected calculations for ^{53}Fe (^{53}Co), in which a prolate $K=19/2$ intrinsic state is obtained by exciting one of the protons (neutrons) from the $[312]5/2$ to the $[303]7/2$ and coupling both to the odd neutron (proton). As in the case of ^{52}Fe , these aligned collective states are favored in energy and become yrast traps.

C. Decay properties of $^{52}\text{Fe}^m$

In this subsection we present theoretical results for the decay of the 12^+ isomeric state. To describe the β^+ decay properties, we used the quenching factor of 0.77 [39] and obtained a half-life of 40 sec, which compares well with the experimental value of 45.94 ± 0.60 sec [12]. The β^+ decay takes place predominantly to the 11^+ state of ^{52}Mn for which the shell model calculations give a branching ratio of 99.7%. The computed $\log ft$ value for this transition, 4.78, agrees nicely with the experimental value of 4.83 ± 0.11 [12].

To study the γ decay of the isomer, it is necessary to compute the $E4$ transitions to the two 8^+ states and the $E6$ transitions to the two 6^+ states. The transitions to the 8_1^+ and 6_1^+ were previously calculated in Ref. [12] using a $(f_{7/2})^n$ model space. The effective charges found in that work differed greatly from those used for the $E2$ transitions. The $E4$ transitions were also calculated including admixtures of other orbitals of the pf major shell using first order perturbation theory. A better agreement with data was obtained in this latter case.

We have calculated the reduced transition probabilities allowing up to a maximum of 6 particles to jump from the $f_{7/2}$ orbit to higher pf orbitals. The effective charges used to reproduce the experimental $E4$ transitions in ^{52}Mn and ^{53}Fe were $e_\pi=0.75$ and $e_\nu=-0.25$. The description of the $E6$ transition in ^{53}Fe required $e_\pi=0.6$ and $e_\nu=-0.4$. These effective charges are similar to those reported in Ref. [12].

We consider, however, that the available experimental data in this mass region is not enough to determine accurately the effective charges and such a theoretical study is beyond the scope of this paper. Therefore, we choose to present our results for the reduced transition probabilities as a function of the effective charges

$$B(E4; 12^+ \rightarrow 8_1^+) = 256(e_\pi + e_\nu)^2 e^2 \text{fm}^8,$$

$$B(E4; 12^+ \rightarrow 8_2^+) = 164(e_\pi + e_\nu)^2 e^2 \text{fm}^8,$$

$$B(E6; 12^+ \rightarrow 6_1^+) = 3.4 \times 10^5 (e_\pi + e_\nu)^2 e^2 \text{fm}^{12},$$

$$B(E6; 12^+ \rightarrow 6_2^+) = 4.6 \times 10^5 (e_\pi + e_\nu)^2 e^2 \text{fm}^{12}, \quad (4)$$

For the partial half-lives we can consider two limits depending on the value of the effective charges. One is given by the effective charges needed in the $E6$ transition on ^{53}Fe and the other by the $E2$ effective charges $e_\pi=1.5$, $e_\nu=0.5$. The ‘‘true’’ effective charges should be somewhere in between. The partial half-lives are then

$$6.3 \times 10^3 \leq T_{1/2}(12^+ \rightarrow 8_1^+) \leq 6.3 \times 10^5 \text{ s},$$

$$2.1 \times 10^5 \leq T_{1/2}(12^+ \rightarrow 8_2^+) \leq 2.1 \times 10^7 \text{ s},$$

$$9.9 \times 10^5 \leq T_{1/2}(12^+ \rightarrow 6_1^+) \leq 9.9 \times 10^7 \text{ s},$$

$$1.8 \times 10^7 \leq T_{1/2}(12^+ \rightarrow 6_2^+) \leq 1.8 \times 10^9 \text{ s}, \quad (5)$$

Comparing these results with the partial β decay half-life computed above, we conclude that the branching ratio for the γ -decay channel of the 12^+ isomeric state of ^{52}Fe is in the range 0.7–0.007%. These values are in agreement with the experimental limit of 0.4% of Ref. [12].

V. CONCLUSIONS

We have investigated high spin states in ^{52}Fe with the 4π spectrometer GASP. Its high detection efficiency and sensitivity allowed us to observe the level scheme up to spin $I=10\hbar$, a fact which was hindered until now by the presence of the 12^+ yrast trap. We could therefore establish experimentally that the retardation of the decay of the 12^+ yrast state is due to its location at an energy lower than that of the 10^+ state.

Four new states, 6_2^+ , 8_1^+ , 8_2^+ , and 10^+ , have been determined, while the spin and parity of other levels have been confirmed. The mean lifetime of five excited states have been measured with the DSAM procedure. Upper limits for the $B(E4)$ reduced transition probabilities for the decay of the 12^+ isomer have been determined experimentally on the basis of the upper limit of its γ -ray decay branching from a previous off-beam measurement [12]. With the new multidetector γ -ray systems, off-beam measurements should now allow determination of such small branchings.

Full pf shell model calculations have been performed for ^{52}Fe , which constitutes the highest mass described so far with the code ANTOINE. The calculated energy levels and the electromagnetic properties, i.e., reduced transition probabilities and lifetimes, are in very good agreement with the data. The difference between the 12^+ states in the cross conjugate nuclei ^{44}Ti and ^{52}Fe can be also satisfactorily explained through shell model calculations. It was concluded that, apart from the lowering of the states due the alignment of the valence nucleons, in ^{52}Fe this state is even lower due to a higher degree of collectivity present in the structure of the wave function related to the contribution of the other orbitals

in the major shell. The evolution of the intrinsic structure of the states with increasing spin has been interpreted by means of a Nilsson projected method. Both calculations, shell model and Nilsson projected method, also describe well the yrast traps known in the $A = 53$ mirror nuclei.

ACKNOWLEDGMENTS

The authors would like to thank B.F. Bayman, A. Poves, D. Rudolph, and A.P. Zuker for fruitful and interesting dis-

cussions. We also thank the crew of the XTU Tandem of the National Laboratory of Legnaro for the smooth operation of the accelerator during the experiment. The computational cycles were provided by the Centro de computación científica de la Facultad de Ciencias at the Universidad Autónoma de Madrid and by the Center for Advanced Computational Research at Caltech. G.M.P. was partly supported by the DGICYES (Spain) and A.G. was supported by the EC under Contract No. ERBCHBGCT940713. This work was partly supported by the grant 3225/1997 of the Romanian Academy of Sciences.

-
- [1] J. A. Cameron, M. A. Bentley, A. M. Bruce, R. A. Cunningham, W. Gelletly, H. G. Price, J. Simpson, D. D. Warner, and A. N. James, *Phys. Rev. C* **49**, 1347 (1994).
- [2] S. M. Lenzi, D. R. Napoli, A. Gadea, M. A. Cardona, D. Hojman, M. A. Nagarajan, C. Rossi Alvarez, N. H. Medina, G. de Angelis, D. Bazzacco, M. E. Debray, M. de Poli, S. Lunardi, and D. De Acuña, *Z. Phys. A* **354**, 117 (1996).
- [3] S. M. Lenzi, C. A. Ur, D. R. Napoli, M. A. Nagarajan, D. Bazzacco, D. M. Brink, M. A. Cardona, G. de Angelis, M. De Poli, A. Gadea, D. Hojman, S. Lunardi, N. H. Medina, and C. Rossi Alvarez, *Phys. Rev. C* **56**, 1313 (1997).
- [4] W. Kutschera, R. B. Huber, C. Signorini, and P. Blasi, *Nucl. Phys.* **A210**, 531 (1973).
- [5] W. P. Alford, R. A. Lindgren, D. Elmore, and R. N. Boyd, *Nucl. Phys.* **A243**, 269 (1975).
- [6] W. Bohne, H. Fuchs, K. Grabisch, D. Hilscher, U. Jahnke, H. Kluge, T. G. Masterson, and H. Morgenstern, *Nucl. Phys.* **A245**, 107 (1975).
- [7] Y. Iritani, J. Kasagi, and H. Ohnuma, *J. Phys. Soc. Jpn.* **43**, 1119 (1977).
- [8] D. Evers, A. Harasim, R. L. McGrath, and W. Assmann, *Phys. Rev. C* **15**, 1690 (1977).
- [9] P. Decowski, W. Benenson, B. A. Brown, and H. Nann, *Nucl. Phys.* **A302**, 186 (1978).
- [10] Huo Junde, *Nucl. Data Sheets* **71**, 659 (1994).
- [11] V. Avrigeanu, D. Bucurescu, G. Constantinescu, E. Dragulescu, M. Ivascu, D. Pantelica, and R. Teodorescu, *Nucl. Phys.* **A272**, 243 (1976).
- [12] D. F. Geesaman, R. L. McGrath, J. W. Noé, and R. E. Malmin, *Phys. Rev. C* **19**, 1938 (1979).
- [13] D. F. Geesaman, R. E. Malmin, R. L. McGrath, J. W. Noé, and J. Cerny, *Phys. Rev. Lett.* **34**, 326 (1975).
- [14] D. Bazzacco, in *Proceedings of the International Conference on Nuclear Structure at High Angular Momentum*, Ottawa, 1992, Report No. AECL 10613, Vol. II, p. 376.
- [15] J. B. Viano, Y. Dupont, and J. Menet, *Phys. Lett.* **34B**, 397 (1971).
- [16] T. Yamazaki, *Nucl. Data* **A3**, 1 (1967).
- [17] M. Abdelrazek *et al.*, University of Tennessee progress report, 1997, p. 12.
- [18] M. Piiparinen, A. Ataç, J. Blomqvist, G. B. Hagemann, B. Herskind, R. Julin, S. Juutinen, A. Lampinen, J. Nyberg, G. Sletten, P. Tikkanen, S. Tormanen, A. Virtanen, and R. Wyss, *Nucl. Phys.* **A605**, 191 (1996).
- [19] NNDC Online Data Service, Brookhaven National Laboratory.
- [20] J. C. Wells and N. R. Johnson, "LINESHAPE: A Computer Program for Doppler-Broadened Lineshape Analysis," Report No. ORNL-6689, 1991, p. 44.
- [21] J. C. Bacelar, A. Holm, R. M. Diamond, E. M. Beck, M. A. Deleplanque, J. Draper, B. Herskind, and F. S. Stephens, *Phys. Rev. Lett.* **57**, 3019 (1986); *Phys. Rev. C* **35**, 1170 (1987).
- [22] F. Brandolini, S. M. Lenzi, D. R. Napoli, R. V. Ribas, H. Somacal, C. A. Ur, D. Bazzacco, J. A. Cameron, G. de Angelis, M. De Poli, A. Gadea, C. Fahlander, S. Lunardi, M. A. Nagarajan, C. Rossi Alvarez, and C. Svensson, *Heavy Ion Phys.* **7**, 113 (1998).
- [23] L. C. Northcliffe and R. F. Schilling, *Nucl. Data Tables* **7**, 233 (1970).
- [24] H. Ejiri and M. J. A. de Voigt, in *Gamma Ray and Electron Spectroscopy in Nuclear Physics*, edited by P. E. Hodgson (Clarendon, Oxford, 1989), Chap. 6.
- [25] E. Caurier, J. L. Egido, G. Martínez-Pinedo, A. Poves, J. Retamosa, L. M. Robledo, and A. P. Zuker, *Phys. Rev. Lett.* **75**, 2466 (1995).
- [26] C. G. Andersson, G. Hellström, G. Leander, I. Ragnarsson, S. Åberg, J. Krumlinde, S. G. Nilsson, and A. Szymański, *Nucl. Phys.* **A309**, 141 (1978).
- [27] J. Vervier, *Nucl. Phys.* **A103**, 222 (1967).
- [28] J. Cerny, J. E. Esterl, R. A. Gough, and R. G. Sextro, *Phys. Lett.* **33B**, 284 (1970).
- [29] D. Seweryniak, I. Ahmad, H. Amro, D. J. Blumenthal, L. T. Brown, M. P. Carpenter, C. N. Davids, S. Fischer, D. J. Henderson, R. V. F. Janssens, T. L. Khoo, C. J. Lister, D. Nisius, T. Davinson, R. J. Irvine, P. J. Woods, W. B. Walters, I. Hibbert, C. Parry, and R. Wadsworth, *Proceedings of the Conference on Nuclear Structure at the Limits*, 1996, ANL, Argonne, 1997 (unpublished), p. 247.
- [30] H. Mang, *Phys. Rev.* **119**, 1069 (1960).
- [31] I. Perlman, F. Asaro, A. Ghiorso, A. Larsh, and R. Latimer, *Phys. Rev.* **127**, 917 (1962).
- [32] A. Faessler, M. Płoszajczak, and K. R. S. Devi, *Phys. Rev. Lett.* **36**, 1028 (1976).
- [33] E. Caurier, A. P. Zuker, A. Poves, and G. Martínez-Pinedo, *Phys. Rev. C* **50**, 225 (1994).
- [34] G. Martínez-Pinedo, A. P. Zuker, A. Poves, and E. Caurier, *Phys. Rev. C* **55**, 187 (1997).
- [35] A. Poves and A. Zuker, *Phys. Rep.* **70**, 235 (1981).
- [36] E. Caurier, code ANTOINE, Strasbourg, 1989 (unpublished).
- [37] R. B. M. Mooy and P. W. M. Glaudemans, *Z. Phys. A* **312**, 59 (1983).
- [38] A. P. Zuker, J. Retamosa, A. Poves, and E. Caurier, *Phys. Rev. C* **52**, R1741 (1995).
- [39] B. H. Wildenthal, M. S. Curtin, and B. A. Brown, *Phys. Rev. C* **28**, 1343 (1983).